Journal of Materials Chemistry A

COMMUNICATION

View Article Online
View Journal | View Issue

Cite this: J. Mater. Chem. A, 2016, 4, 7601

Received 20th February 2016
Accepted 19th April 2016

DOI: 10.1039/c6ta01514j

www.rsc.org/MaterialsA

Integrating photovoltaic conversion and lithium ion storage into a flexible fiber†

Hao Sun,[a] Yishu Jiang,[a] Songlin Xie,[a] Ye Zhang,[a] Jing Ren,[a] Abid Ali,[a] Seok-Gwang Doo,[b] In Hyuk Son,[b] Xianliang Huang[c] and Huisheng Peng*[a]

Flexible electronics has witnessed the rapid advancement of fiber-shaped energy devices, particularly fiber-shaped integrated devices that simultaneously realize energy conversion and storage in a single fiber. However, it remains challenging to produce integrated energy fibers with enhanced energy storage capacities and output voltages, and meanwhile retain the high flexibility and integration. Here, we demonstrate a novel family of integrated energy devices by integrating photoelectric conversion and lithium ion storage into a flexible fiber. The fiber-shaped integrated energy device exhibits a core–sheath structure with the photoelectric conversion part at the sheath and the lithium ion storage part at the core. It simultaneously displays a high energy storage capacity and output voltage. The integrated energy fibers are lightweight, flexible and weavable, and represent promising candidates to power the next-generation portable and wearable electronic devices. The results presented here could provide inspiration for the development of high-performance integrated devices.

Flexible and wearable electronics is inspiring scientists to design and fabricate various powering systems with high flexibility and integration.[1] To this end, fiber-shaped energy harvesting and storage devices are particularly promising due to the combined advantages of being lightweight, flexible and weavable compared with the conventional planar or blocky structures.[2–9] Fiber-shaped solar cells,[10–14] supercapacitors[15–19] and lithium-ion batteries[20,21] have been intensively explored in recent years. Generally, two fiber electrodes coated with active materials were wound together to produce a fiber-shaped energy harvesting or conversion device. In order to further reduce the size and enrich functionality, it is necessary to integrate the photoelectric conversion and electrochemical storage into a single fiber-shaped device. Some efforts have thus been made to integrate a dye-sensitized or polymer solar cell and a supercapacitor typically by sharing a fiber electrode.[22–25] However, the electrochemical storage part has been fully charged by the photoelectric conversion part within a few seconds due to the low energy density of the supercapacitor part. In addition, the output voltages are obviously too low to power various electronic devices for practical applications.

In this communication, we have developed a novel family of energy devices by integrating photoelectric conversion and lithium ion storage into a flexible fiber. The fiber-shaped integrated energy device (FIED) shows a core–sheath structure with the photoelectric conversion (PC) part at the sheath and the lithium-ion storage (LS) part at the core. It simultaneously displays a high photoelectric conversion efficiency and energy storage capability, with an output voltage up to 2.6 V to power the next-generation electronic devices.

The fabrication process of the FIED is schematically illustrated in Fig. 1. Briefly, $LiMn_2O_4$ (LMO) and $Li_4Ti_5O_{12}$ (LTO) nanoparticles were incorporated with aligned multi-walled carbon nanotube (MWCNT) fibers *via* a biscrolling method, serving as positive and negative electrodes of the LS part, respectively. A layer of the gel electrolyte was coated onto aligned MWCNT/LMO and MWCNT/LTO fibers, followed by wrapping on a rubber fiber (diameter of 500 μm) (Fig. 1a) and encapsulating into a heat-shrinkable tube (diameter of ~1.5 mm) to complete the LS part (Fig. 1b). An aligned MWCNT sheet was then wrapped on the surface of the above heat-shrinkable tube (Fig. 1c). Separated PC segments were formed by the use of paper masks prior to the wrapping process (Fig. 1d). The following fiber was then inserted into spring-shaped photoanodes (Fig. 1e), followed by injection of the

[a]State Key Laboratory of Molecular Engineering of Polymers, Department of Macromolecular Science and Laboratory of Advanced Materials, Fudan University, Shanghai 200438, China. E-mail: penghs@fudan.edu.cn

[b]Energy Materials Lab, Materials Research Center, Samsung Advanced Institute of Technology, Samsung Electronics Co., Ltd, 130 Samsung-ro, Suwon-si, Gyeonggi-do, 443803, South Korea

[c]Samsung R&D Institute China, Beijing 100028, China

† Electronic supplementary information (ESI) available: Experimental techniques, schematic illustration of the cross-sectional structure of the device, TEM images of $LiMn_2O_4$ and $Li_4Ti_5O_{12}$ nanoparticles, current density–voltage curve of a photovoltaic conversion unit, photograph of multi-walled carbon nanotube (MWCNT)/$Li_4Ti_5O_{12}$ and MWCNT/$LiMn_2O_4$ hybrid electrodes wrapped on a rubber fiber at original and bending states are included in Fig. S1 to S6. See DOI: 10.1039/c6ta01514j

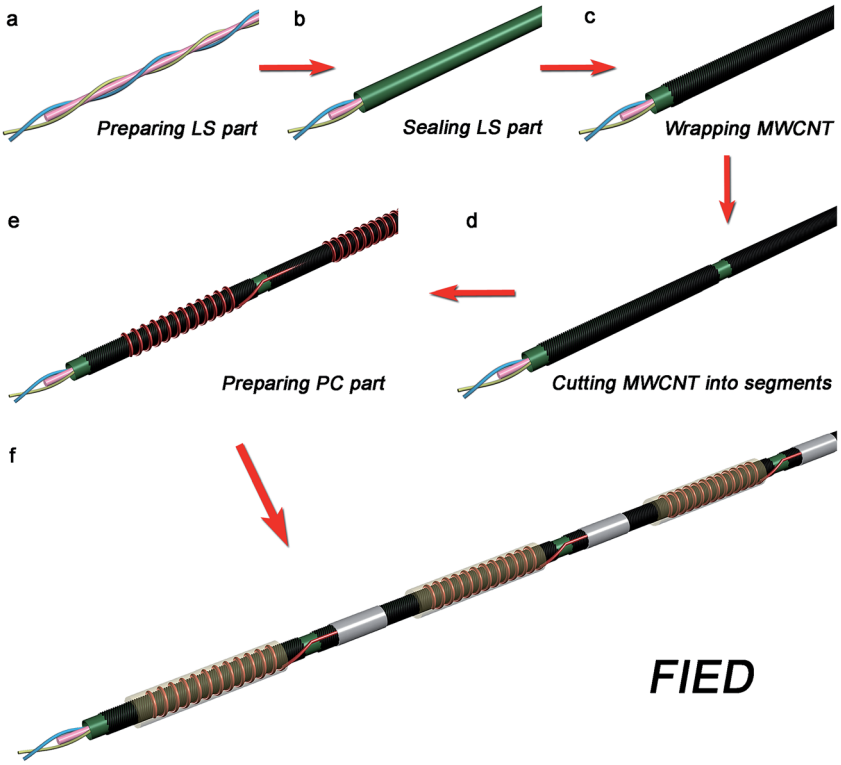

Fig. 1 Schematic illustration to the fabrication process of the fiber-shaped integrated energy device (FIED).

liquid electrolyte and encapsulation of each PC unit in one heat-shrinkable tube, and the overall diameter of the FIED was measured to be ~2.5 mm. The output voltage of the PC part should be higher than the charging voltage of the LS part. To this end, several neighbouring PC units were connected by MWCNT sheets with the assistance of silver paste (Fig. 1f). The resulting FIED shows a core–sheath structure with the PC unit at the sheath and the LS part in the core (Fig. S1†). The integration of LS was used to achieve high energy storage capability.

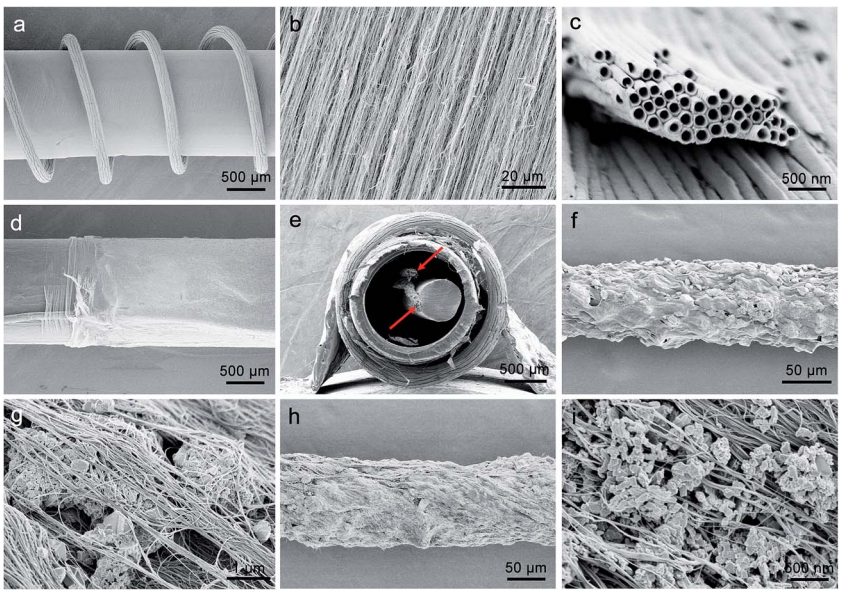

Fig. 2 SEM images of the structure of the FIED. (a) Spring-shaped photoanode on a plastic tube (aligned MWCNT sheet being wrapped on the surface). (b) and (c) Aligned MWCNT sheet and titanium dioxide nanotubes, respectively. (d) Joint point of two neighboring PC units. The aligned MWCNT sheet was wrapped on the outer surface to fasten the Ti wire. (e) Cross-sectional image of an FIED with the two arrows indicating two fiber electrodes. (f) and (g) Aligned MWCNT/LMO fiber at low and high magnifications, respectively. (h) and (i) Aligned MWCNT/LTO fiber at low and high magnifications, respectively.

Fig. 2a shows a typical scanning electron microscopy (SEM) image of the PC part. The MWCNT remained highly aligned to favor a rapid charge transport on the electrode (Fig. 2b). Titanium dioxide nanotube arrays were perpendicularly grown on the surface of the spring-shaped titanium wire (screw pitch of ~1 mm) *via* an anodic oxidation method (Fig. 2c). A close contact between the MWCNT sheet and Ti wire was found at the connecting point of the neighboring unit due to the use of silver paste that was filled in the voids to reduce the contact resistance (Fig. 2d). A cross-sectional SEM image demonstrated a core–sheath structure with the twisted MWCNT/LMO and MWCNT/LTO fibers in the LS core (Fig. 2e). Aligned MWCNTs served as a conductive scaffold to provide a low electrical resistance, while LMO and LTO were well dispersed within MWCNT bundles to provide high energy storage capability (Fig. 2f–i). The MWCNT/LTO hybrid electrode was further coated with a thin layer of graphene oxide to enhance the structural stability of the electrode.[21] No binder, conducting diluent and metal current collector were required, making the FIED lightweight.

The photovoltaic conversion and energy storage properties were carefully investigated and presented in Fig. 3. A single PC unit demonstrated a power conversion efficiency of 6.05% with an open-circuit voltage of 0.68 V (Fig. S3†). Importantly, the open-circuit voltage was about 7.5 times of a single one, *i.e.*, 5.12 V, at a unit number of 8 with the same short-circuit current of ~200 μA (Fig. 3a). The overall optical status can be enhanced by adopting some efficient strategies, for instance, introducing a diffusion reflector or a micro-light concentrating groove at the PC part, which can increase the output power.[26] For the LS part, the voltage profiles in charging and discharging at a current of 0.02 mA showed a high coulombic efficiency of over 95% (Fig. 3b). The discharging plateau voltage was increased from 2.2 to 2.5 V with decreasing discharging currents from 0.05 to 0.01 mA, indicating a stable operation of the LS part at a variety of discharging currents (Fig. 3c). A high mass specific capacity of 112 mA h g^{-1} had been achieved at 0.01 mA; it was determined by the MWCNT/LTO electrode and may be further enhanced by increasing the amount of active materials or being replaced with the other electrodes. The specific capacity had been maintained at 88% after 100 charging/discharging cycles with a coulombic efficiency of almost 100% (Fig. 3d).

A switch was incorporated between the PC and LS parts to realize the photocharging and discharging processes. Under illumination, the switch was turned on and the dye molecules on the photoanode of the PC part were excited to the excited state, followed by injecting electrons to the conduction band of titanium dioxide,[27] and the LS part was charged by the PC part. During the discharging process, the switch between the PC and LS parts was turned off, and the LS part began to discharge to the external circuit. The output voltage from the PC part should exceed the charging voltage plateau of the LS part, so the PC parts with increasing repeating units of 5, 6, 7 and 8 had been studied and compared. They were photocharged under the illumination of simulated AM1.5 solar light and discharged at 0.05 mA when the output voltage reached 3.3 V (Fig. 4a). For 5 units, the voltage of the LS part rapidly exceeded 2.5 V and suffered from a very slow increase to below 3.3 V for more than 600 s. Even when the LS part was discharged at 3 V, the voltage had been rapidly decreased to 1.5 V without a typical discharging plateau, indicating an unsuccessful photocharging process due to a low photovoltage. In the case of 6 units, a successful photocharging process had been achieved, which was certified by a more rapid increase in voltage from 1.5 to 3.3 V within 150 s and an obvious discharging plateau. The photocharging time had been further reduced to 115 and 86 s for 7 and 8 units, respectively (Fig. 3a). Note that the photocharging voltage was also affected by the electrical resistances of PC and LS parts. Due to the resistance of the PC part, the

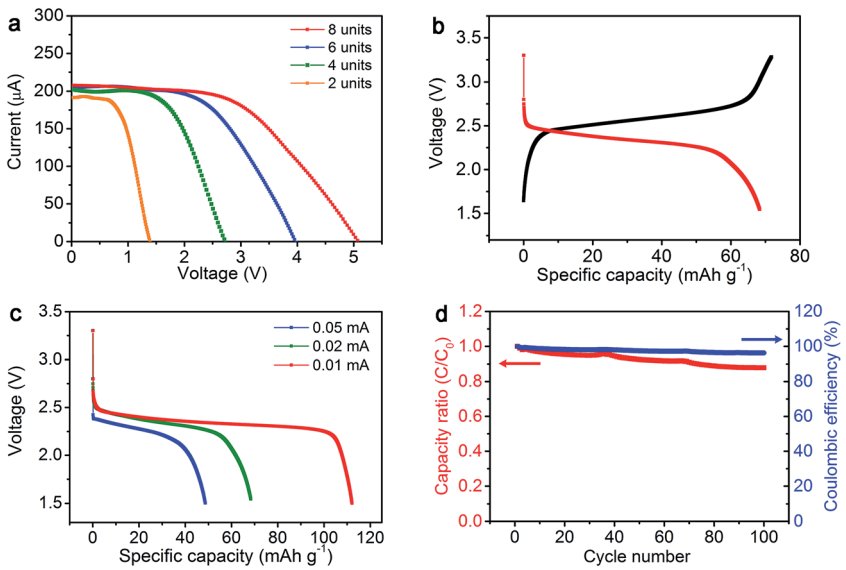

Fig. 3 (a) Current–voltage curves of PC parts with increasing unit numbers. (b) Charging and discharging profiles of an LS part at a current of 0.02 mA. (c) Discharging curves of an LS part with increasing currents from 0.01 to 0.05 mA. (d) Cyclic performance of an LS part during 100 charging/discharging cycles.

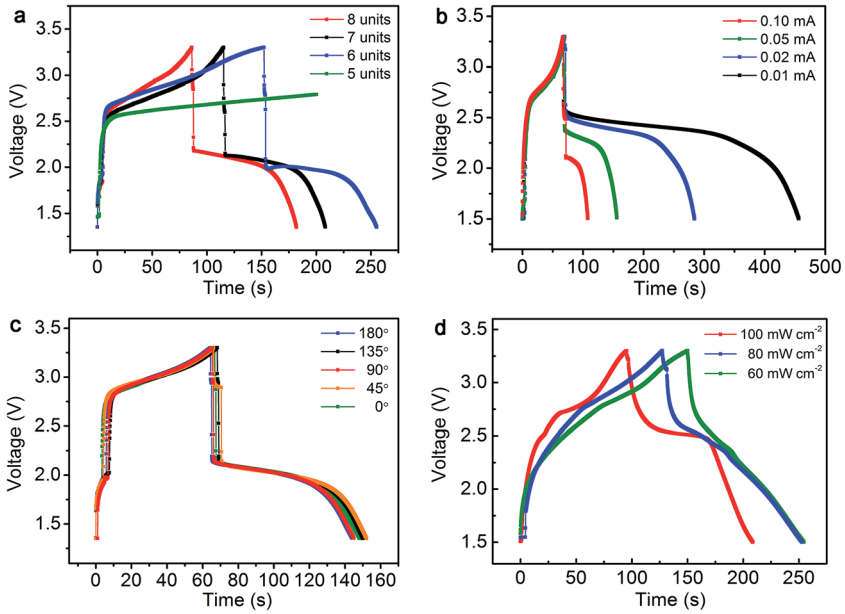

Fig. 4 Photocharging and discharging performances of the FIED. (a) Photocharging and discharging curves with increasing PC units. The photocharging process was performed under the illumination of simulated AM1.5 solar light (100 mW cm^{-2}). Discharging current, 0.05 mA. (b) Photocharging and discharging curves with eight PC units with increasing discharging current. (c) Photocharging and discharging curves at different angles of incident light. Discharging current, 0.05 mA. (d) Photocharging and discharging curves with different power densities of incident light. Discharging current, 0.05 mA.

actual charging voltage for the LS part was lower than the open-circuit voltage of the PC part. The total photoelectric conversion and energy storage efficiency had been increased with the increasing PC unit, attributed to a combined effect of a decrease in charging time and an increase in the effective photoanode area. Once fully photocharged, the FIED can discharge at a variety of currents from 0.01 to 0.1 mA (Fig. 4b). A high energy density of ~22 W h kg^{-1} (~15.3 W h cm^{-3}) had been achieved, one to two orders of magnitude larger compared with previous reports based on supercapacitors, as well as a comparable power density of ~800 W kg^{-1} (~0.54 W cm^{-3}). The energy and power densities are also higher than those of planar lithium thin-film batteries (1–10 mW h cm^{-3} and 10^{-2} to 10^{-3} W cm^{-3}).[28]

As expected, the photocharging and discharging curves of the FIED remained almost unchanged with the increasing angle of incident light from 0 to 180° because the power conversion efficiencies at the PC part were independent of the incident angle based on the fiber shape (Fig. 4c). Therefore, the FIED can harvest light from various directions and is particularly suitable for indoor applications with abundant scattered light. The dependence of photocharging and discharging performance on incident light intensity was also investigated (Fig. 4d). With decreasing light intensity from 100 to 60 mW cm^{-2}, the photocharging time of an FIED containing eight PC units was increased from 95 to 150 s, attributed to decreased photogenerated current and voltage of the PC part. The specific capacities were well maintained with a fluctuation below 10%. The independence of the performance on the light intensity provides advantages in many fields, *e.g.*, for wearable applications under weak light.

The FIED was lightweight (Fig. 5a) and flexible (Fig. 5b), so it can be readily woven for smart clothes that can harvest light and store it at daytime, and discharge to power electric devices at night. As a demonstration, a smart glove was fabricated based on the FIED and used to power two light emitting diodes connected in parallel. Upon illumination, light was converted to electric energy and stored in the LS part (Fig. 5c). When discharging in the dark, the stored electrochemical energy was converted to electric energy to light up the light emitting diodes (Fig. 5d).

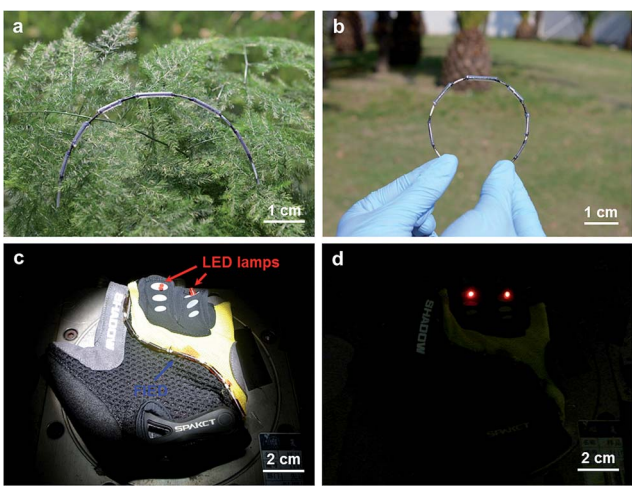

Fig. 5 (a) and (b) Photographs of an FIED model product on the leaves and under bending, respectively. (c) and (d) Photographs of an FIED being woven into a sport glove for photocharging (under AM1.5 illumination) and powering two light emitting diodes in the dark, respectively.

The liquid electrolyte is used in the PC part which requires a careful encapsulation to avoid possible leakage, so a solid-state one can be designed to solve this problem for practical applications.[29,30] Similarly, the currently used switch may be inconvenient for practical applications, and a microelectronic chip containing a voltage detector can be incorporated for smart control. When the voltage of the LS part exceeds the set value, the circuit between the PC and LS parts can be automatically cut off. The energy storage performance of the integrated system can be increased by incorporating more active materials into the fiber electrode. For instance, an extended discharge time was realized by using ~5 times more electrode materials at the LS part, and represented an ~5-time enhancement on the capacity at the same current (Fig. S5†); the discharge plateau can be raised from 2.2 to 2.6 V by incorporating amorphous carbon (25 wt%) into the MWCNT/LMO composite electrode to enhance the rate performance, accompanied by a decrease in the capacity (Fig. S6†).[31] The other rechargeable fiber-shaped energy storage devices with higher capacity such as a lithium sulphur battery can be also used to enhance the energy storage.[32] More efforts are underway to further improve the energy harvesting and storage performance.

In summary, a new fiber-shaped integrated device that can simultaneously and effectively realize energy conversion and storage is developed by making the photoelectric conversion at the sheath and lithium ion storage at the core. Both high photovoltages up to 5.12 V and high output voltages up to 2.6 V are achieved to power various electronic devices. It is lightweight, flexible and weavable, and represents a promising candidate to support the next-generation portable and wearable electronics. A variety of integrated energy and electronic devices may be also produced on the basis of the same strategy by incorporating lithium ion batteries or other batteries.

Acknowledgements

This work was supported by NSFC (21225417, 51573027, 51403038), STCSM (15XD1500400, 12nm0503200, 15JC1490200) and the Program for Outstanding Young Scholars from Organization Department of the CPC Central Committee. This work was supported in part by the Samsung Advanced Institute of Technology (SAIT)'s Global Research Outreach (GRO) Program (IO140919-02248-01).

Notes and references

1 D. Schmidt, M. Hager and U. Schubert, *Adv. Energy Mater.*, 2016, **6**, 1500369.
2 D. Yu, K. Goh, H. Wang, L. Wei, W. Jiang, Q. Zhang, L. Dai and Y. Chen, *Nat. Nanotechnol.*, 2014, **9**, 555–562.
3 S. Pan, J. Deng, G. Guan, Y. Zhang, P. Chen, J. Ren and H. Peng, *J. Mater. Chem. A*, 2015, **3**, 6286–6290.
4 H. Sun, H. Li, X. You, Z. Yang, J. Deng, L. Qiu and H. Peng, *J. Mater. Chem. A*, 2013, **2**, 345–349.
5 Q. Meng, H. Wu, Y. Meng, K. Xie, Z. Wei and Z. Guo, *Adv. Mater.*, 2014, **26**, 4100–4106.
6 K. Wang, Q. Meng, Y. Zhang, Z. Wei and M. Miao, *Adv. Mater.*, 2013, **25**, 1494–1498.
7 L. Kou, T. Huang, B. Zheng, Y. Han, X. Zhao, K. Gopalsamy, H. Sun and C. Gao, *Nat. Commun.*, 2014, **5**, 3754.
8 J. Zhong, Q. Zhong, Q. Hu, N. Wu, W. Li, B. Wang, B. Hu and J. Zhou, *Adv. Funct. Mater.*, 2015, **25**, 1798–1803.
9 J. Zhong, Y. Zhang, Q. Zhong, Q. Hu, B. Hu, Z. L. Wang and J. Zhou, *ACS Nano*, 2014, **8**, 6273–6280.
10 Z. Yang, H. Sun, T. Chen, L. Qiu, Y. Luo and H. Peng, *Angew. Chem., Int. Ed.*, 2013, **52**, 7545–7548.
11 H. Sun, Z. Yang, X. Chen, L. Qiu, X. You, P. Chen and H. Peng, *Angew. Chem., Int. Ed.*, 2013, **125**, 8434–8438.
12 X. Fan, Z. Chu, F. Wang, C. Zhang, L. Chen, Y. Tang and D. Zou, *Adv. Mater.*, 2008, **20**, 592–595.
13 D. Zou, D. Wang, Z. Chu, Z. Lv and X. Fan, *Coord. Chem. Rev.*, 2010, **254**, 1169–1178.
14 S. Hou, X. Cai, H. Wu, X. Yu, M. Peng, K. Yan and D. Zou, *Energy Environ. Sci.*, 2013, **6**, 3356–3362.
15 J. Lee, M. Shin, S. Kim, H. Cho, G. Spinks, G. Wallace, M. Lima, X. Lepró, M. Kozlov and R. Baughman, *Nat. Commun.*, 2013, **4**, 1970.
16 H. Sun, X. You, J. Deng, X. Chen, Z. Yang, J. Ren and H. Peng, *Adv. Mater.*, 2014, **26**, 2868–2873.
17 G. Sun, X. Zhang, R. Lin, J. Yang, H. Zhang and P. Chen, *Angew. Chem., Int. Ed.*, 2015, **127**, 4734–4739.
18 K. Jost, D. Durkin, L. Haverhals, E. Brown, M. Langenstein, H. De Long, P. Trulove, Y. Gogotsi and G. Dion, *Adv. Energy Mater.*, 2015, **5**, 1401286.
19 T. Chen, R. Hao, H. Peng and L. Dai, *Angew. Chem., Int. Ed.*, 2015, **54**, 618–622.
20 Y. Kwon, S. Woo, H. Jung, H. Yu, K. Kim, B. Oh, S. Ahn, S. Lee, S. Song and J. Cho, *Adv. Mater.*, 2012, **24**, 5192–5197.
21 J. Ren, Y. Zhang, W. Bai, X. Chen, Z. Zhang, X. Fang, W. Weng, Y. Wang and H. Peng, *Angew. Chem., Int. Ed.*, 2014, **53**, 7864–7869.
22 T. Chen, L. Qiu, Z. Yang, Z. Cai, J. Ren, H. Li, H. Lin, X. Sun and H. Peng, *Angew. Chem., Int. Ed.*, 2012, **51**, 11977–11980.
23 Z. Yang, J. Deng, H. Sun, J. Ren, S. Pan and H. Peng, *Adv. Mater.*, 2014, **26**, 7038–7042.
24 Y. Fu, H. Wu, S. Ye, X. Cai, X. Yu, S. Hou, H. Kafafy and D. Zou, *Energy Environ. Sci.*, 2013, **6**, 805–812.
25 Z. Zhang, X. Chen, P. Chen, G. Guan, L. Qiu, H. Lin, Z. Yang, W. Bai, Y. Luo and H. Peng, *Adv. Mater.*, 2014, **26**, 466–470.
26 Y. Fu, Z. Lv, S. Hou, H. Wu, D. Wang, C. Zhang, Z. Chu, X. Cai, X. Fan and Z. L. Wang, *Energy Environ. Sci.*, 2011, **4**, 3379–3383.
27 A. Hagfeldt, G. Boschloo, L. Sun, L. Kloo and H. Pettersson, *Chem. Rev.*, 2010, **110**, 6595–6663.
28 D. Pech, M. Brunet, H. Durou, P. H. Huang, V. Mochalin, Y. Gogotsi, P. L. Taberna and P. Simon, *Nat. Nanotechnol.*, 2010, **5**, 651–654.
29 D. Wang, S. Hou, H. Wu, C. Zhang, Z. Chu and D. Zou, *J. Mater. Chem.*, 2011, **21**, 6383–6388.
30 N. Zhang, J. Chen, Y. Huang, W. Guo, J. Yang, J. Du, X. Fan and C. Tao, *Adv. Mater.*, 2016, **28**, 263–269.
31 D. Cericola, P. Novák, A. Wokaun and R. Kötz, *J. Power Sources*, 2011, **196**, 10305–10313.
32 X. Fang, W. Weng, J. Ren and H. Peng, *Adv. Mater.*, 2016, **28**, 491–496.